A Computational Navier-Stokes Fluid-Dynamics-Simulation Study of Wormhole Propagation in Carbonate-Matrix Acidizing and Analysis of Factors Influencing the Dissolution Process

Olatokunbo O. Akanni and **Hisham A. Nasr-El-Din,** Texas A&M University;
and **Deepak Gusain,** Carbo Ceramics Incorporated

Summary

This study demonstrates the application of an alternative numerical-simulation approach to effectively describe the flow field in a two-scale carbonate-matrix-acidizing model. The modified model accurately captures the dissolution regimes that occur during carbonate-matrix acidizing. Sensitivity tests were performed on the model to compare the output with experimental observations and previous two-scale models in the literature. A nonlinear reaction-kinetics model for alternative acidizing fluids is also introduced.

In this work, the fluid-field flow is described by the Navier-Stokes momentum approach instead of Darcy's law or the Darcy-Brinkman approach used in previous two-scale models. The present model is implemented by means of a commercial computational-fluid-dynamics (CFD) package to solve the momentum, mass-conservation, and species-transport equations in Darcy scale. The software is combined with functions and routines written in the C programming language to solve the porosity-evolution equation, update the pore-scale parameters at every timestep in the simulation, and couple the Darcy and pore scales.

The output from the model simulations is consistent with experimental observations, and the results from the sensitivity tests performed are in agreement with previously developed two-scale models with the Darcy approach. The simulations at very-high injection rates with this model require less computational time than models developed with the Darcy approach. The results from this model show that the optimal injection rate obtained in laboratory coreflood experiments cannot be directly translated for field applications because of the effect of flow geometry and medium dimensions on the wormholing process. The influence of the reaction order on the optimal injection rate and pore volumes (PVs) of acid required to reach breakthrough is also demonstrated by simulations run to test the applicability of the model for acids with nonlinear kinetics in reaction with calcite.

The new model is computationally less expensive than previous models with the Darcy-Brinkman approach, and simulations at very-high injection rates with this model require less computational time than Darcy-based models. Furthermore, the possibility of extending the two-scale model for acid/calcite reactions with more-complex chemistry is shown by means of the introduction of nonlinear kinetics in the reaction equation.

Introduction

Matrix stimulation of wells with acid is a widely used practice to enhance the inflow of hydrocarbon to the wellbore. This process involves injecting an acidizing fluid into the formation, below the formation-fracture pressure, to recover or improve the permeability of the rock matrix near the wellbore. In carbonate reservoirs, the acidizing fluid is injected to create conductive-flow channels that bypass any formation damage or region of low permeability near the wellbore, thereby increasing the inflow performance of the well. The post-treatment skin factor of carbonate reservoirs could be negative (if the flow channels penetrate past the damage zone in the formation), signifying an improvement over the original skin factor. These conductive-flow channels created by the acid in carbonate formations are known as wormholes.

Dominant wormholes are formed in an acid-dissolution process during a carbonate-matrix-acidizing treatment if the acidizing fluid is injected at an optimal rate. The acid flows preferentially to the regions of least resistance, such as the larger interconnected pores (high permeability), rapidly dissolving the matrix material in its path. As the flow paths receive an increasing portion of the acidizing fluid during the process, the length and volume of the pores increase, eventually becoming wormholes (Fredd and Fogler 1998). Wormhole patterns do not necessarily form in the dissolution of carbonate rock with an acid; the dissolution structure is mainly dependent upon the injection rate and fluid-mineral properties, which include the reaction kinetics, mass-transfer rates, flow geometry, formation heterogeneity, and fluid-loss rate (Hung et al. 1989; Buijse 2000; Fredd and Miller 2000). The dissolution patterns that can be formed during carbonate-matrix acidizing are face dissolution, conical wormholes, dominant wormholes, ramified wormholes, and uniform dissolution.

At very-low injection rates in laboratory coreflood tests, the acidizing fluid is consumed at the inlet-flow face of the core before it can penetrate the rock, resulting in face dissolution. A high volume of the fluid is then required to reach breakthrough at the outlet. At slightly higher injection rates, a conical-shaped dissolution channel is formed as greater amounts of the acidizing fluid are consumed on the walls of the flow channels, and the fluid penetrates into the rock and enlarges flow channels. At an optimal injection rate, the fluid is transported to the tip of the evolving flow channel and propagates the channel, which then leads to the formation of a dominant wormhole. At injection rates higher than the optimal rate, the fluid is forced into smaller pores and the dissolution channels become more branched, resulting in ramified wormholes (Fredd and Miller 2000). At very-high rates, the fluid penetrates into the matrix but is not completely spent because of insufficient residence time, which leads to uniform dissolution patterns and unsuccessful treatment in field conditions.

Original SPE manuscript received for review 2 October 2015. Revised manuscript received for review 23 May 2017. Paper (SPE 187962) peer approved 18 July 2017.

The dissolution pattern affects the skin evolution because it determines the depth of penetration of the acid into the rock. When dominant wormhole patterns are formed, the acid penetrates deepest into the formation, which leads to the highest reduction in skin after treatment. Therefore, to obtain the best results from an acid-stimulation treatment, it is important to inject the acid at the optimal injection rate for the particular fluid/mineral system.

Numerous studies have been conducted to understand the propagation of wormholes during carbonate-matrix acidizing. From these studies, mathematical models were developed to predict the dissolution structure of the acid/rock reaction, the optimal injection rate for the most efficient treatment, and/or the propagation rate of the wormhole in the rock with volume injected to monitor the skin evolution during treatment.

The accuracy of existing carbonate-matrix-acidizing models in estimating the optimal injection rate, wormhole-propagation rate, and type of dissolution structure formed has been examined in Akanni and Nasr-El-Din (2015). The main limitation of those models is in the translation of the results from the core scale to field scale, which includes correlation of flow geometry, inclusion of formation heterogeneities, and wormhole competition in field conditions. Other shortcomings are the constraint of dissolution patterns to the wormholing regimes in most of the existing carbonate-matrix-acidizing models and the nonfactoring of the effect of additives on the acidizing-fluid-dissolution rate.

In this work, a two-scale model—with fluid flow described by the Navier-Stokes momentum approach—is used to study the propagation of wormholes during carbonate acidizing. This model is demonstrated to effectively capture all dissolution regimes. Sensitivity tests were performed on the model to investigate and quantify how various factors, such as flow geometry, initial average porosity, medium heterogeneity, core dimensions, and reaction kinetics, affect the wormholing process at the optimal injection rate, and the amount of acid injected to reach breakthrough. Results from a nonlinear kinetics model are examined for the extension of the two-scale model for acidizing fluids with complex chemistry in their reaction with calcite.

Literature Review

Brief reviews of some carbonate-acidizing models in literature can be found in Schechter (1992), Golfier et al. (2002), Panga et al. (2005), and Glasbergen et al. (2009). A more extensive review and validation of carbonate-acidizing models was made by Fredd and Miller (2000), in which the authors classified the mathematical models into five categories depending on the approach to solution, and this was later extended to seven categories by Akanni and Nasr-El-Din (2015). These categories are the capillary-tube approach, Damköhler-number approach, transition-pore theory, network models, Péclet-number approach, semiempirical approach, and two-scale (averaged continuum) models. Some models are derived from more than one of the approaches listed, with the Damköhler-number theory being the most often combined.

In the capillary-tube approach, the wormhole is modeled as a cylindrical tube. The early models derived from this approach simulated mass-transfer-limited dissolution by use of bundles of capillary tubes (Rowan 1959) with a focus on the effect of fluid leakage and the mechanism of transport and reaction in the wormhole. Schechter and Gidley (1969) extended this theory to include the effects of pore-merging surface-reaction-limited dissolution. Hung et al. (1989, 1997), Wang et al. (1993), and Buijse (2000) have also developed models derived from this approach. A fundamental limitation of these models is that the assumption of the initial formation of dominant wormholes and, thus, microscopic-pore distribution (number of pores and radii on rock surface where acid is injected) is required to set up the model.

Studies by Hoefner and Fogler (1988) show that the Damköhler number controls the wormhole-formation process. The effect of the Damköhler number on the wormhole structure was investigated and confirmed by their experimental work. The Damköhler number is defined as the ratio of the net rate of acid dissolution to the rate of transport of acid by convection. Fredd and Fogler (1998, 1999) conducted further studies on the effects of transport and reaction on the formation of wormholes for a wide range of fluid systems, including strong acids, weak acids, and chelating agents. They showed that these fluid systems are influenced by a variety of transport and reaction processes, and when both processes are taken into account, a common dependence on the Damköhler number is observed. An optimal Damköhler number of approximately 0.29 was found for all the fluid/mineral systems they investigated. The models derived from the Damköhler-number theory need to be combined with other models to predict skin evolution because they do not independently predict wormhole growth. Wormhole density and dimensions are required because the Damköhler number only applies to a single wormhole for a linear coreflood test, and the results do not translate directly to field scale.

The transition-pore theory was originally developed by Wang et al. (1993) to calculate the optimal flux to generate dominant wormholes during a matrix-acid treatment. They postulated that a critical pore cross-sectional area exists on the face of the rock for the formation of wormholes. An expression was obtained from the growth-rate functions, by use of previous work by Schechter and Gidley (1969), which relates the optimal acid flux with the Damköhler number and emphasizes the effects of rock mineralogy, reaction temperature, and acid concentration. This method requires microscopic-pore description for implementation. It cannot be applied for monitoring skin evolution during treatment, and it incorrectly predicts that an increase in acid concentration will decrease the optimal acid flux. Huang et al. (1997) included a fluid-loss model with the transition-pore theory to translate the results from laboratory-core scale to field scale, but the model exhibits the same basic limitations also observed in the Wang et al. (1993) model.

Other researchers have used the network approach to describe processes in porous media where the important structural property of pore interconnectedness must be included. It was first introduced by Fatt (1956) and, according to Hoefner and Fogler (1988), has been used successfully to include fluid displacement (Simon and Kelsey 1972), relative permeability (Rose 1957), and dispersion in porous media (Sahimi et al. 1990). Hoefner and Fogler (1988) performed a theoretical study on the dissolution of porous media by flowing acid with this approach, and also combined their work with experimental observations. Fredd and Fogler (1998) extended the works of Bryant et al. (1993) and Thompson and Fogler (1997) on a 3D physically representative network model to simulate the effects of transport and reaction on the formation of wormholes. The network models require enormous computational power to translate to field or laboratory scale, making them unavailable for practical application.

Daccord et al. (1989) first presented the Péclet-number-theory model as one that quantifies wormholes by their equivalent hydraulic length. This method is dependent on correlations at the scale of the core sample itself. The physical parameters involved in the problem are introduced as dimensionless numbers. The model postulates that the propagation of wormholes is a function of the Péclet number, injection volume, and a fractal dimension. In developing the growth-rate equation for the radial case, it is assumed that the effect of a finite wellbore radius is equivalent to pumping an extra volume of fluid equal to that necessary to obtain a penetration equal to the wellbore radius. Frick et al. (1994) extended the work of Daccord et al. (1989) by also considering wormholes as fractals. The influences of acid volume, injection rate, fractal dimension, porosity, and the ratio of undamaged to damaged permeability on well performance are factored in. The results of their study incorrectly suggest that the injection rate has no major effect on the dissolution patterns.

Buijse and Glasbergen (2005) developed a semiempirical approach to capture the essential physics and chemistry of wormhole propagation in carbonates, in which the growth rate of the wormhole front was modeled as a function of the interstitial velocity of the acid. Parameters such as permeability, mineralogy, temperature, and acid concentration are not modeled explicitly, but are incorporated into the model in the form of two constants calculated from the optimal acid velocity and PV to breakthrough at this velocity. These constants are obtained from coreflood tests for the fluid/mineral system being investigated. In developing a radial analog of the linear wormhole model, it is assumed that the functional relationship between the interstitial velocity and the velocity of the wormhole front as observed in coreflood tests holds for radial geometry. Furui et al. (2012) extended this approach and combined it with the previously described capillary-tube model (Hung et al. 1989), which is dependent on acid transport and fluid loss from a single wormhole. This model improves on the original by accounting for the effect of core dimensions used in the coreflood test, from which the parameters used in the model are obtained. Wormhole growth is related to the in-situ injection velocity at the tip of the dominant wormhole, and at sufficiently high injection velocity, the acid concentration at the wormhole tip is assumed to be equal to the acid concentration (at injection point). The effective surface area available for the acid reaction is assumed to be proportional to the wormhole-penetration length. The results of this model depend on the efficiency of the coreflood experiments, from which the main parameters used in the equations are obtained.

In the two-scale (averaged-continuum) approach, the transport and reaction of the acidizing fluid is modeled as an interaction between the Darcy scale and the pore scale. Liu et al. (1997) developed a Darcy-scale coupled fluid-flow simulator for sandstones, which was extended for the dissolution of carbonates by Golfier et al. (2002). The modified model uses a mass-transfer coefficient that is calculated from a pore-scale simulation at each stage in the simulation of the model, thereby coupling the pore-scale phenomena to the Darcy scale. The model assumes a complete mass-transfer-controlled reaction and is shown to capture qualitative and quantitative features of dissolution in the mass-transfer-controlled regime. Panga et al. (2002, 2005) and Ghommem et al. (2015) later developed a two-scale continuum model, which captures the reaction and transport mechanisms for describing wormhole formation in carbonates. Kalia and Balakotaiah (2007) built on the work by Panga et al. (2005) and Ghommem and Brady (2015) to simulate radial flow in the model. Kalia and Balakotaiah (2009) studied the effect of heterogeneities of the porous medium on the dissolution patterns formed during a carbonate-acidizing process by use of the two-scale model.

Further work by Maheshwari et al. (2012) was performed to extend the two-scale model for 3D simulation. This model was extended to be made applicable for gelled acids by Ratnakar et al. (2012), in which the two-scale model is combined with a semiempirical rheological model that accounts for viscosity as a function of pH value, shear rate, and temperature. Maheshwari et al. (2014) also applied this approach to emulsified acids. Various investigators have used other applications of the two-scale approach. De Oliveira et al. (2012) used the model to investigate the effect of mineralogical heterogeneity on the amount of acid injected as a function of injection rates. Liu et al. (2012) examined the effect of normally distributed porosities on wormholing patterns, and Zhang et al. (2014) studied wormhole-propagation behavior and its effect of acid leakoff in acid fracturing with the two-scale model.

The two-scale models give a good prediction of the dissolution pattern for the fluid/mineral systems mentioned. They can also provide an estimation of the optimal injection rate for laboratory-scale experiments but will require enormous computational power to be applicable for field-scale simulation. For emulsified acid, the model does not account for emulsion-droplet-size distribution, and it is assumed that the droplets are very fine and will be unchanged as the acid propagates through the rock. For gelled acid, the model does not account for polymer adsorption at the pore walls. First-order irreversible reactions are assumed for the kinetics in these models, which makes them inapplicable for acidizing fluids with more-complex reaction kinetics with carbonates.

Model Description

A detailed description of the development of the two-scale model is presented in Panga et al. (2002, 2005). The flow field is given by Darcy's law in their model, but in the present study, the flow field is described by the Navier-Stokes momentum approach. The equations for the Darcy- and pore-scale models are presented here.

Darcy-Scale Equations. The fluid-flow field is given by the Navier-Stokes equation:

$$\frac{\partial(\rho\mathbf{u})}{\partial t}+\nabla\cdot(\rho\mathbf{u}\mathbf{u})=-\nabla p-\frac{\mu}{\mathbf{K}}\mathbf{u}, \quad \ldots\ldots (1)$$

where $\mathbf{u}$ is the superficial-velocity vector, ρ is the fluid density, $\mathbf{K}$ is the permeability tensor, and p is pressure. The continuity equation, Eq. 2, derived from the mass balance of fluids, accounts for the effect of local volume change during dissolution on the flow field:

$$\frac{\partial\varepsilon}{\partial t}+\nabla\cdot\mathbf{u}=0. \quad \ldots\ldots (2)$$

The Darcy-scale description of the transport of acid species, from fluid-phase balance of reacting species, is given by

$$\frac{\partial(\varepsilon C_f)}{\partial t}+\mathbf{u}\cdot\nabla C_f=\nabla\cdot(\varepsilon\boldsymbol{D}_e\cdot\nabla C_f)-k_c a_v(C_f-C_s), \quad \ldots\ldots (3)$$

where ε is the porosity of the medium, C_f is the original concentration of the acid in the fluid phase, C_s is the concentration of the acid at the fluid/solid interface, $\boldsymbol{D}_e$ is the effective dispersion tensor, k_c is the local mass-transfer coefficient, and a_v is the interfacial area available for reaction per unit volume of the medium. The reaction kinetics in Eq. 4 balance the amount of acid transferred from the fluid phase to the surface to the amount reacted at the surface:

$$k_c(C_f-C_s)=R(C_s). \quad \ldots\ldots (4)$$

The porosity-evolution equation, derived from the balance between the solid dissolved and fluid consumed, is given by

$$\frac{\partial\varepsilon}{\partial t}=\frac{R(C_s)a_v\alpha}{\rho_s}, \quad \ldots\ldots (5)$$

where $R(C_s)$ represents the reaction kinetics, ρ_s is the density of the rock, and α is the dissolving power of the acid. Eqs. 1 through 5 are the Darcy-scale-model equations, as described by Panga et al. (2005). For a first-order reaction, the kinetics equation can be written as $R(C) = k_s C_s$ (where k_s is the dissolution-rate constant), and then Eq. 4 is modified to

$$C_s = \frac{C_f}{\left(1 + \frac{k_s}{k_c}\right)}. \quad \ldots\ldots (6)$$

Pore-Scale Equations. The porosity of the rock increases as the acid propagates and dissolves part of the solid phase. This transformation results in changes of pore-scale properties such as permeability, pore radius (r_p), and interfacial surface area per unit volume. The relationships between these rock properties and porosity are adapted from the Carman-Kozeny correlation and are given by the following pore-scale equations (Panga et al. 2005; Carman 1937):

$$\frac{\mathbf{K}}{\mathbf{K}_o} = \frac{\varepsilon}{\varepsilon_o}\left[\frac{\varepsilon(1-\varepsilon_o)}{\varepsilon_o(1-\varepsilon)}\right]^{2\beta}, \quad \ldots\ldots (7)$$

$$\frac{\boldsymbol{r}_p}{\boldsymbol{r}_o} = \left[\frac{\varepsilon(1-\varepsilon_o)}{\varepsilon_o(1-\varepsilon)}\right]^{\beta}, \quad \ldots\ldots (8)$$

and

$$\frac{\boldsymbol{a}_v}{\boldsymbol{a}_o} = \left(\frac{\varepsilon}{\varepsilon_o}\right)\left[\frac{\varepsilon(1-\varepsilon_o)}{\varepsilon_o(1-\varepsilon)}\right]^{-\beta}, \quad \ldots\ldots (9)$$

where β is the pore-structure-relation constant. The local mass-transfer and effective-dispersion coefficients are obtained by use of the following correlations (Gupta and Balakotaiah 2001; Balakotaiah and West 2002):

$$Sh = \frac{2\boldsymbol{k}_c r}{D_m} = Sh_\infty + 0.7 Re_p^{1/2} Sc^{1/3}, \quad \ldots\ldots (10)$$

$$\boldsymbol{D}_{eX} = \alpha_{os} D_m + \frac{2\lambda_X \|\mathbf{u}\| r}{\varepsilon}, \quad \ldots\ldots (11)$$

$$\boldsymbol{D}_{eT} = \alpha_{os} D_m + \frac{2\lambda_T \|\mathbf{u}\| r}{\varepsilon}, \quad \ldots\ldots (12)$$

where Sh is the Sherwood number or dimensionless mass-transfer coefficient; Sh_∞ is the asymptotic Sherwood number; Re_p is the Reynolds number defined by $Re_p = t\frac{2\|\mathrm{u}\| r}{v}$; Sc is the Schmidt number given by $Sc = \frac{v}{D_m}$; v is the kinematic viscosity; α_{os} is a constant that depends on the structure of the porous medium (pore connectivity); D_{eX} is the longitudinal-dispersion coefficient; D_{eT} is the transverse-dispersion coefficient in the y- and z-direction; and λ_X and λ_T are constants that depend on the structure of the medium (λ_X is approximately 0.5 and λ_T is approximately 0.1 for a packed bed of spheres). These correlations account for both diffusive and convective contributions (Maheshwari and Balakotaiah 2013).

The correlation equations are valid for both developing and fully developed laminar and turbulent flow in porous media, as presented in Panga et al. (2002). The first term in the dispersion-correlation equations (Eqs. 11 and 12) represents the molecular-diffusion contribution and the second term represents the convection contribution to dispersion (Ratnakar et al. 2012). The diffusion contribution is dominant for small pores and very-low Reynolds numbers, whereas the convective contribution is dominant for larger pores at higher Reynolds numbers.

Flow-Field Description. In the Liu et al. (1997) and Golfier et al. (2002) averaged-continuum models, the fluid-flow field was described by the Darcy-Brinkman approach to accurately predict the flow field when the Reynolds number is greater than unity and the viscous contribution to the flow is significant (Panga et al. 2002). The flow in both the porous media (wormholes and vugs) and the fluid itself are represented in this approach. However, various investigators have shown that Darcy's law can be used to effectively approximate fluid flow in the two-scale model and is computationally less expensive than the Darcy-Brinkman approach.

In the two-scale model used in this study, the fluid flow is described by the Navier-Stokes approach. De Oliveira et al. (2012) used this approach in their two-scale model to study the effect of mineralogical heterogeneity on wormhole patterns, but the dissolution regimes at very-low injection rates were not presented in their work. Like the Darcy-Brinkman approach, the Navier-Stokes approach allows a natural transition between flow in porous media and in wormholes and vugs and is also computationally less expensive than the Darcy-Brinkman approach.

The Navier-Stokes momentum approach effectively models free flow in vugs and wormholes, and especially flow at very-high injection rates where the effect of viscous contribution to flow is accentuated. This novel approach, as shown in the next section, reduces to Darcy's law at low flow rates to model flow in porous medium. The results from this study, compared with previous reports, show that the computational time required to complete simulation in the ramified- and uniform-dissolution regimes (high injection rates) is considerably reduced with fluid flow described by the Navier-Stokes approach instead of Darcy's law.

Model Implementation

To run the simulations of the described two-scale model with the Navier-Stokes approach, Fluent (ANSYS 2015), a commercial CFD software package, is used to solve the momentum, mass-continuity, and transport equations in the Darcy scale.

In the software, the equation for conservation of mass, or the continuity equation, is written as

$$\frac{\partial \rho}{\partial t} + \nabla \cdot (\rho \mathbf{u}) = S_m, \quad \ldots\ldots (13)$$

where source S_m is the mass added to the continuous phase from the dispersed second phase and any user-defined source in the software. Eq. 13 is the general form of the mass-conservation equation for incompressible and compressible flows, from which Eq. 2 for the incompressible flow in this model is derived.

The conservation-of-momentum equation is written in Fluent in the general form:

$$\frac{\partial}{\partial t}(\rho\mathbf{u}) + \nabla\cdot(\rho\mathbf{u}\mathbf{u}) = -\nabla p + \nabla\cdot(\tau) + \rho\boldsymbol{g} + \boldsymbol{F}, \quad (14)$$

where $\boldsymbol{\tau}$ is the stress tensor, $\rho\boldsymbol{g}$ is the gravitational body force, and $\boldsymbol{F}$ is the sum of external body forces, which also contains other model-dependent source terms such as porous-media and user-defined sources. For the momentum approach, the equation used in this model to describe fluid flow (Eq. 1), the gravitational force is ignored and the stress tensor is not included because the momentum source (the last term in Eq. 1) accounts for viscous effects.

The momentum-source term added to Eq. 14 is used to model porous media. The general source term in Fluent is composed of two parts as given in Eq. 15: the viscous-loss term (Darcy, the first term on the right-hand side of the equation), and an inertial-loss term (the second term on the right-hand side of the equation).

$$S = -\left(\frac{\mu}{\mathbf{K}}\mathbf{u} + C_2\frac{1}{2}\rho|\mathrm{u}|\mathbf{u}\right), \quad (15)$$

where S is the momentum-source term and C_2 is the inertial-resistance factor. In laminar flow through porous media, the pressure drop is typically proportional to velocity and the inertial part of the source term is negligible. Ignoring convective acceleration and diffusion, the Navier-Stokes approach for the porous media model (Eq. 1) then reduces to Darcy's law:

$$\nabla p = \frac{\mu}{\mathbf{K}}\mathbf{u}. \quad (16)$$

The transport equation is written by user-defined codes in the CFD software adapted for this model. This is combined with functions and routines written in the C programming language to solve the porosity-evolution equation, update the pore-scale parameters at every timestep, and to couple the pore scale with the Darcy scale. **Fig. 1** gives the work flow of the simulation showing the sequence of equations solved in the model.

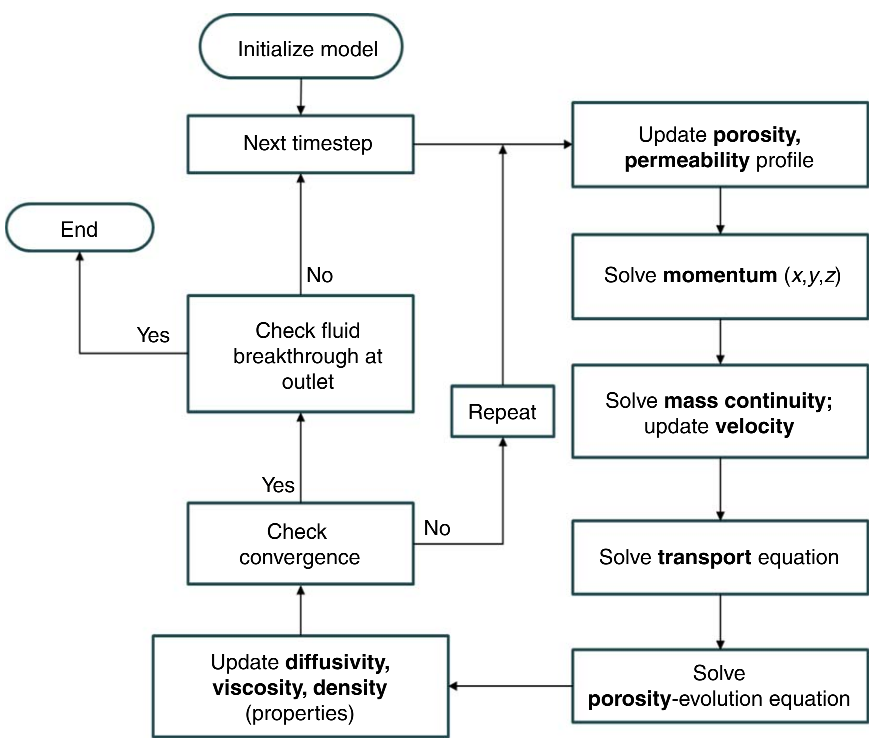

Fig. 1—The simulation work flow showing the sequence of solutions and properties updates.

The model is started by assigning the porosity values to individual cells in the numerical domain. The simulation starts by updating the porosity distribution in the cells and corresponding permeability values from the adapted Carman-Kozeny correlation in Eq. 7. Next, momentum equations for *u, v,* and *w* velocities are solved sequentially, followed by mass continuity and velocity updates (Eqs. 1 and 2). Subsequently, the transport equation (Eq. 3) is solved, followed by the porosity-evolution equation (Eq. 5) to calculate the change in porosity as the acid species are transported across the cells. The fluid properties in the cells are then updated with the new species distribution. Fluent then checks for convergence or additional iterations before moving on to the next timestep. This continues until fluid breakthrough is estimated to occur at the outlet of the core.

The simulations are run at the Texas A&M University High Performance Research Computing facility to take advantage of parallel-processing capabilities. In the dominant wormholing regime, the computational time is nearly 3 to 4 hours, but the time taken to reach breakthrough in the ramified- and uniform-dissolution regimes (high injection rates) is lower than that. At very-low injection rates (face-dissolution regime), the computational time is in days.

Base Case. The base case is modeled to simulate the acidizing-coreflood tests of 0.5 M hydrogen chloride (HCl) on calcite-core samples using the experimental work of Fredd and Fogler (1998). In the simulation study for the 3D model, the numerical-mesh domain is a 4-in.-long cylindrical shape with a 1.5-in. diameter. The grid cells are made of 400,000 hexahedral and quadrilateral cells. For the 2D case, the numerical-mesh domain is rectangular with a dimension of 1.5×4 in. and made up of 110,000 quadrilateral grid cells.

Table 1 gives the values of the parameters used in the base case of this simulation study. Most of these parameters are obtained from the experimental work of Fredd and Fogler (1998) and the simulation study by Maheshwari and Balakotaiah (2013). The experiments were conducted at 23°C.

Parameter	Value
Acid diffusivity (D_m)	3.6×10^{-9} m^2/s
Acid-dissolving power (α)	50 kg/kmol
Acid viscosity (μ)	0.001 kg/m·s
Asymptotic Sherwood number (Sh_∞)	3.66
Average porosity (ε_o)	0.2
Constant in dispersion correlations (α_{os})	0.5
Constant in axial-dispersion correlation (λ_X)	0.5
Constant in transverse-dispersion correlation (λ_T)	0.1
Initial average permeability ($\mathbf{K}_o$)	1×10^{-15} m^2
Initial interfacial area per unit volume (a_o)	5000 m^{-1}
Initial mean pore size (r_o)	1 μm
Pore-structure-relation constant (β)	1
Porosity-heterogeneity magnitude ($\Delta\varepsilon_o$)	±0.1
Rock density (ρ_s)	2710 kg/m^3
Surface-dissolution reaction-rate constant (k_s)	0.002 m/s

Table 1—Values of parameters used in numerical simulations of the base model (Fredd and Fogler 1998; Maheshwari and Balakotaiah 2013).

At very-low rates (face-dissolution regime), the number of grid cells must be increased to effectively capture the dissolution at these regimes. According to Maheshwari and Balakotaiah (2013), approximately 160 million grid cells will be required to effectively capture face dissolution for the mesh-domain size of $1.5 \times 1.5 \times 4$-in. rectangular parallelepiped domain, which is similar to the cylindrical domain of 1.5-in. diameter by 4-in. length used in this study.

As expected, more computational run time for the program will be required to complete the simulation at very-low injection rates because the dissolution takes place at a slower rate and more of the rock will be dissolved in the face-dissolution regime. In addition, because a high number of grid cells is required to accurately capture the dissolution pattern at these regimes, the simulation runs at a much-slower rate in real time, which means more computational time will be needed. Unfortunately, there are limited high-performance-computing licenses available for parallel computing with the CFD software at the Texas A&M University High Performance Research Computing facility to practically run simulations at face-dissolution regimes for this large computational-mesh domain and high number of grid cells.

The current solution to this limitation is to use a smaller mesh domain to capture and demonstrate the dissolution patterns at the conical- and face-dissolution regimes. The domain is reduced by a factor of five for the 3D and 2D linear cases with the number of grid cells kept the same. The PVs-to-breakthrough (PV_{BT}) results for the larger domain are compared qualitatively with those of the smaller domain at and above the optimal injected rates, and this is extended for rates less than the optimal injection rate. Information on other domain sizes used in this work to study the radial flow and the effect of medium dimensions on the acid-efficiency curve will be provided in the discussion of results.

Numerical-Solution Scheme. A control-volume-based technique is used to solve the momentum-conservation and transport equations in the Darcy scale of the two-scale model. The equations are converted to algebraic equations that are then solved numerically with the finite-volume method.

On the basis of recommendations from the Fluent users guide (ANSYS 2015), a pressure-implicit-with-splitting-of-operators pressure-velocity coupling scheme is used, with neighbor and skewness correction to improve efficiency. A least-squares cell-based spatial-discretization method is used for constructing the fluid-concentration values at the cell faces with a second-order upwind scheme, and a quadratic upstream interpolation for convective kinematics scheme is used for the momentum term.

The timestep size for the numerical simulation is varied between 0.1 and 0.01 seconds, depending on the dissolution regime. The lower timestep size is used at the conical- and face-dissolution regimes. The maximum number of iterations per timestep is set at 20. The number of iterations was fewer than 20, with the average number of iterations ranging from 10 to 15; tolerance was 0.001. Lower flow rates required more iterations.

Initial and Boundary Conditions. For wormholes to be started in the carbonate rock, there must be some heterogeneity in the porous medium. This condition is introduced in this model in the form of porosity heterogeneity. The average porosity of the base case is 0.2 with a heterogeneity of 50%, which means the values in the porosity-distribution profile range from 0.1 to 0.3. A least-squares interpolation method is then used to assign the porosity values from the generated profile to individual grid cells in the numerical domain. **Fig. 2** shows the initial porosity distribution for the different domain cases used in this study. Other initial conditions are zero velocity field in the medium and zero acid concentration.

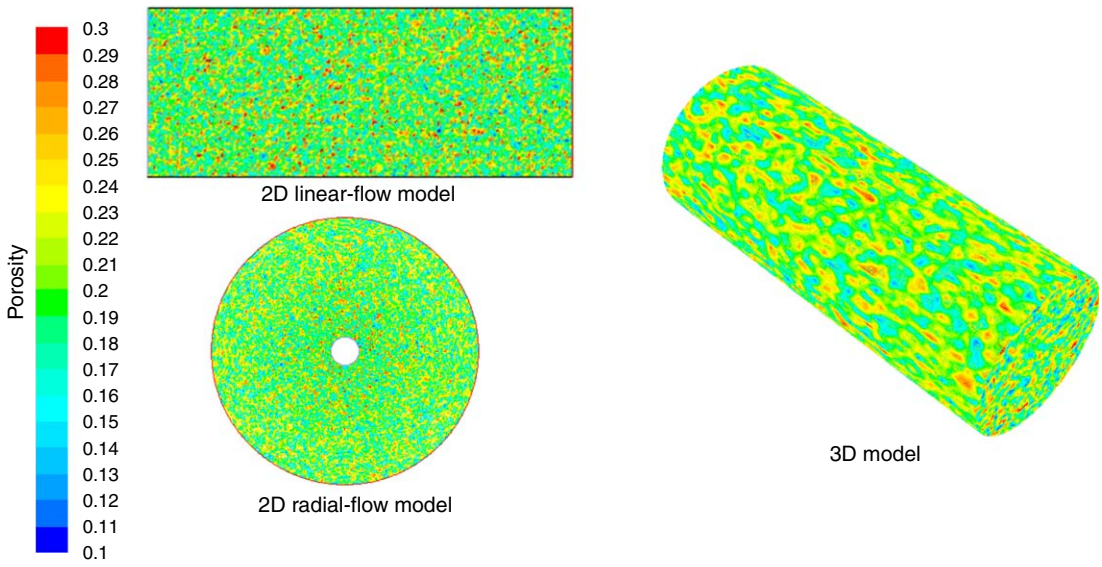

Fig. 2—The initial porosity profile of domain cases used in this study.

The boundary condition at the core inlet is a constant injection velocity, depending on the input for the particular simulation run, and a concentration of 0.5 M HCl. At the core outlet, the acid flux and the pressure are set to zero. Neither the flow nor acid flux occurs across the boundary at the perimeter of the domain.

Results and Discussion

The results of sensitivity-test simulations performed in this study are presented mainly in the form of acid-efficiency curves. This output plots the PV_{BT} vs. the injection rate or velocity. From these curves, the optimal injection rate and the minimum PV_{BT} values for the conditions being investigated can be observed. The breakthrough time of acid at the outlet of the core in the numerical simulation occurs when the pressure drop across the porous medium drops to 1/100 of its initial value (Kalia and Balakotaiah 2009).

Wall-Clock Run Time for Program at High Injection Rates. The computational run time at high injection rate in this model is lower than the reported time from previous two-scale models. The Darcy's-law-based model by Maheshwari et al. (2012) and Maheshwari and Balakotaiah (2013) were run on personal-computer clusters, and their reported computational time at very-high injection rate using Darcy's-law-based models is in days. This is significantly higher than the simulation time of less than 3 hours required for similar cases at very-high injection rate by the Navier-Stokes-based model used in this study. Furthermore, high-injection-rate simulations with this model were run on standalone computers, and the computational time was fewer than 24 hours.

2D and 3D Linear-Flow Model. The results from the 2D and 3D flow models are presented here. The dissolution patterns from a 2D simulation model with linear flow are displayed in **Fig. 3** using the porosity contour of the numerical simulation of the coreflood-acidizing process. The output shows that the model effectively captures the dissolution patterns in carbonate acidizing and also shows the effect of injection rate on the type of dissolution pattern formed.

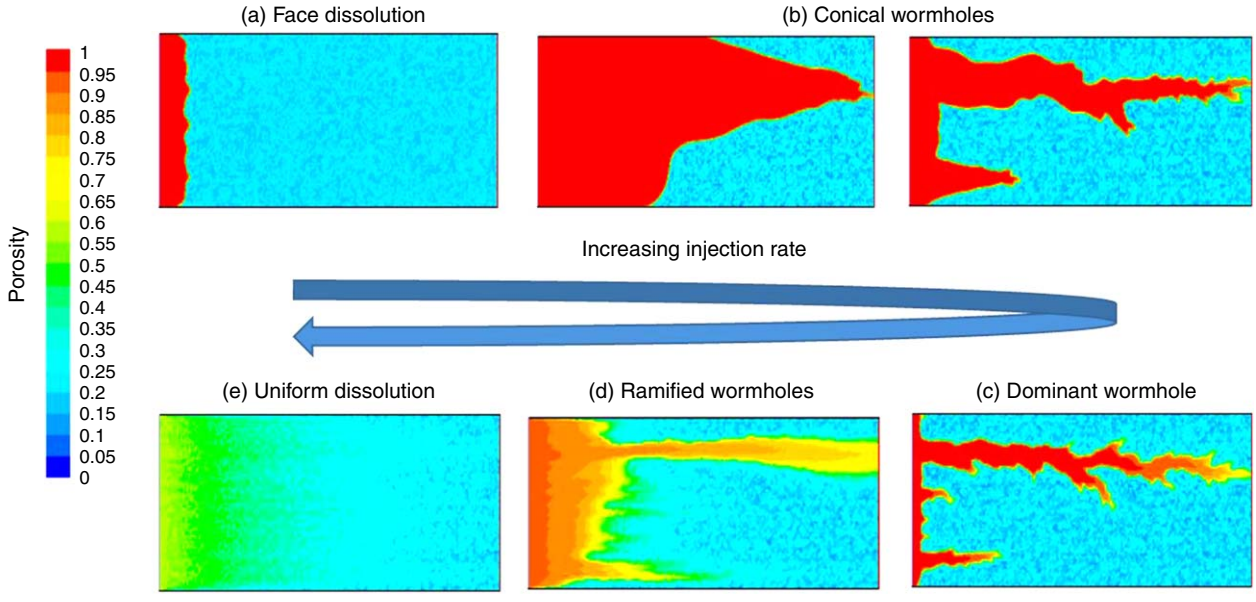

Fig. 3—Porosity contour showing the dissolution patterns obtained from injection rates ranging from a minimum of 3.23×10^{-6} m/s to a maximum of 0.323 m/s (to capture all possible dissolution patterns) from the 2D linear-flow model.

Fig. 4 presents the acid-efficiency curve from the 2D linear-flow model. The semilog plot of the acid-efficiency curve shows that, at low injection rates, a large amount of acid is required to reach breakthrough at the outlet of the porous medium. Face dissolution occurs at these rates, and the acid will have to completely dissolve the solid phase before fluid breakthrough is observed at the exit of the core. The amount of acid to breakthrough decreases as the injection rate increases until it reaches an optimal injection rate, at which minimum PV_{BT} occurs. The amount of acid required to reach breakthrough gradually increases at rates greater than the optimal injection rate. The PV_{BT} is observed to increase with the acid-injection rate (Q) as $Q^{1/3}$, which is similar to the experimental results reported by Frick et al. (1994) and Bazin (2001). At very-high injection rates (in the uniform-dissolution regime), the slope of the plot is observed to change from one-third to unity. This correlation of the acid-injection rate and PV_{BT} values greater than the optimal injection rate was also reported by simulation studies conducted by Maheshwari and Balakotaiah (2013).

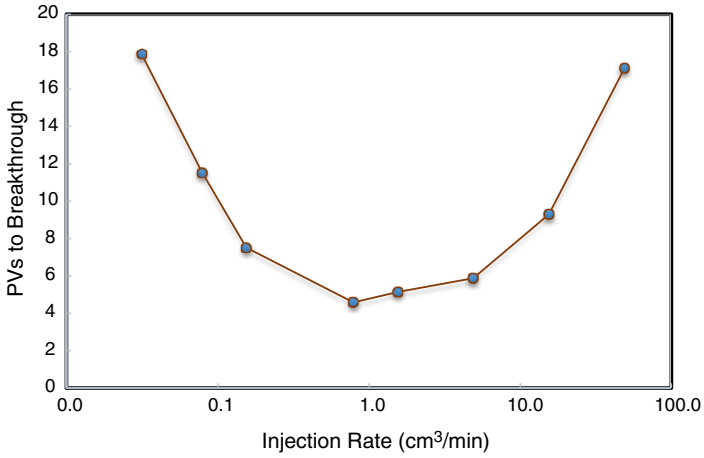

Fig. 4—The acid-efficiency curve of the 2D numerical simulation with linear flow showing the effect of the injection rate on the volume of acid required to reach breakthrough.

The output from the numerical simulation of the 3D linear-flow model, showing the various dissolution regimes, is presented in **Fig. 5,** and the patterns are similar to experimentally observed dissolution images reported in previous studies (Hoefner and Fogler 1988; Fredd and Fogler 1998; Fredd and Miller 2000). The dissolution process and the effect of injection rate on wormhole formation in the 3D model are similar to those in the 2D model. The optimal injection rate obtained from the simulation of the base case in this 3D model is 1.1 cm^3/min, which is in the optimal rate range of 1 to 2 cm^3/min of the same fluid/mineral system obtained from coreflood experiments by Fredd and Fogler (1998). The PV_{BT} at the optimal rate from this numerical simulation is 1.2, which is close to the unity PV_{BT} value observed in the Fredd and Fogler (1998) experiments. Maheshwari and Balakotaiah (2013) also reported an optimal injection rate of 1.92 cm^3/min from their simulation studies and a corresponding PV_{BT} value close to unity.

Fig. 6 shows the comparison of the acid-efficiency curves from the 2D and 3D models. The compared output from this study follows the expected qualitative trend in a previous study (Panga et al. 2005). The plot shows that the amount of acid required to reach breakthrough in the wormhole regimes and the optimal injection rate are higher in the 2D model than in the 3D model. The difference in PV_{BT} values is because in the 2D model, the wormhole volume is the wormhole surface in two discretized directions multiplied by the depth of the domain in the third undiscretized direction, and this volume is greater than the wormhole volume in the 3D model (Cohen et al. 2008). In intermediate wormhole regimes, acid channeling rapidly bypasses a significant portion of the pore space and acid velocity goes to essentially zero away from the dominant wormhole channels. For a similar wormhole structure, the PV not contacted by acid is higher in the 3D model, resulting in a lower PV_{BT} in the 3D model than in the 2D model. This effect is similar to that observed in cases with higher cross-sectional flow area, as shown in a later subsection examining the effect of aspect ratio on PV_{BT} values. The PV_{BT} values at the face- and uniform-dissolution regimes are independent on the dimension of the model because spatial gradients do not appear in the asymptotic limits (Panga et al. 2005).

Effect of Flow Geometry. To investigate the effect of flow geometry on the acid-efficiency curve, a 2D radial-flow model was developed for comparison with the 2D linear-flow model with the same aspect ratio. The 2D domain is a circular mesh with an external radius of 0.79 in. and an internal radius of 0.079 in. The mesh is made up of 110,000 quadrilateral grid cells. The acid-injection inlet is at the internal radius, and the fluid propagates radially toward the external radius until breakthrough is observed at the boundary. The dissolution patterns from radial flow appear similar to the patterns from the linear-flow model **(Fig. 7).**

Fig. 8 shows the comparison of the acid-efficiency curves from the radial- and linear-flow models. Fig. 8 shows that the optimal injection rate in the radial-flow model is higher than that of linear flow. The optimal injection rate in the radial-flow model is higher because the injection velocity decreases with the increasing domain radius as the wormholes propagate in the medium (Kalia and Glasbergen 2009). The radial-flow model yields wormholes that are thinner and feature more enhanced branching than those in the linear-flow model. Thus, the PV_{BT} at the optimal injection rate in the radial-flow model is lower than that of the linear model. These results are consistent with observations from previous studies (Frick et al. 1994; Cohen et al. 2008).

Effect of Initial Average Porosity. To study the effect of initial average porosity on wormhole propagation, three 2D linear-flow cases of initial average porosity values of 0.1, 0.2, and 0.3, all with the same porosity heterogeneity range of 50%, were simulated. **Fig. 9** shows the dissolution patterns at the optimal injection rate. The plot shows that the higher the initial average porosity of the medium, the larger the wormhole diameter because of more fluid loss along the walls of the wormhole. **Fig. 10** gives the acid-efficiency curves, highlighting the amount of acid injected to reach breakthrough for the three cases.

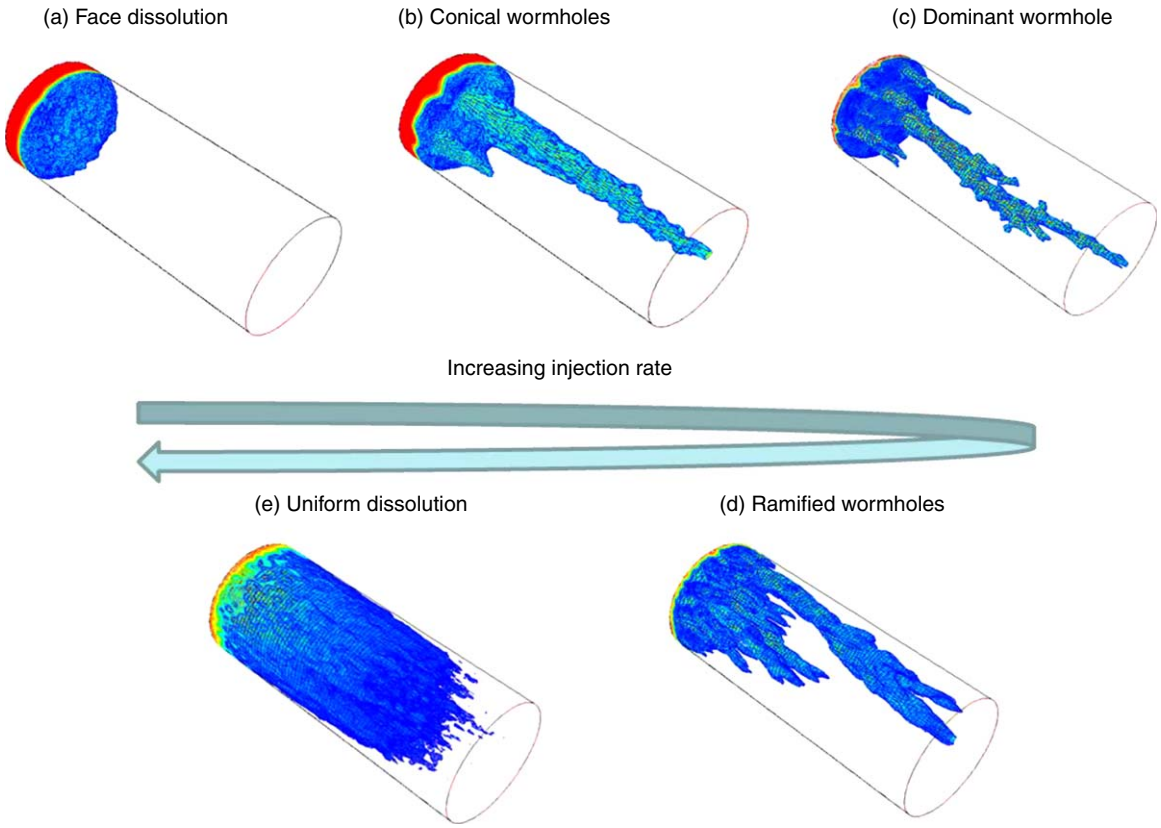

Fig. 5—Dissolution patterns from the numerical simulation of the 3D linear-flow-model contour from injection rates ranging from a minimum of 0.01 cm^3/s to a maximum of 98 cm^3/s.

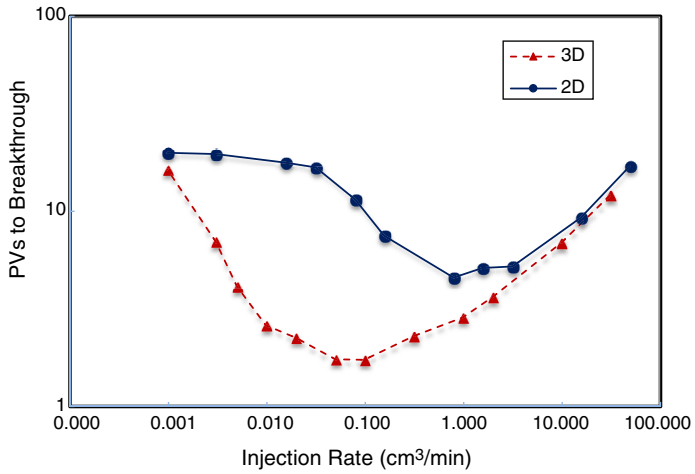

Fig. 6—Comparison of the acid-efficiency curves from the numerical simulation of 2D and 3D models.

In the face-dissolution regime, a higher amount of acid is required to reach breakthrough for cases with lower initial average porosity values. Complete dissolution of the rock occurs in this regime, and the lowest-porosity case will require the most amount of acid to reach breakthrough because of the highest percentage of solid phase in the medium. In the intermediate regime, the acid injected to breakthrough is higher for cases with higher initial average porosity because of the formation of wider wormholes, as previously explained. At high injection rates, increased fluid loss in the medium occurs for cases with high initial porosity, requiring more acid to reach a certain factor of increase in permeability than for low-initial-porosity cases.

Effect of Porosity Distribution. The path of wormhole propagation is determined by the porosity distribution and heterogeneity magnitude in the carbonate rock. The porosity distribution in this model is randomly generated and the effect of this distribution on wormholing and the amount of acid injected to breakthrough is examined by creating four cases with the same average porosity of 0.2 and heterogeneity of 50%, but different porosity-distribution profiles. **Fig. 11** shows the wormhole-propagation patterns from the four cases with different porosity distribution, and **Fig. 12** presents the acid-efficiency curves of the simulation results of these cases. The plot in Fig. 12 shows that the porosity distribution has some effect on the PV_{BT} values at and greater than the optimal injection rate (approximately 0.8 cm^3/min), but no effect at rates lower than the optimal injection rate.

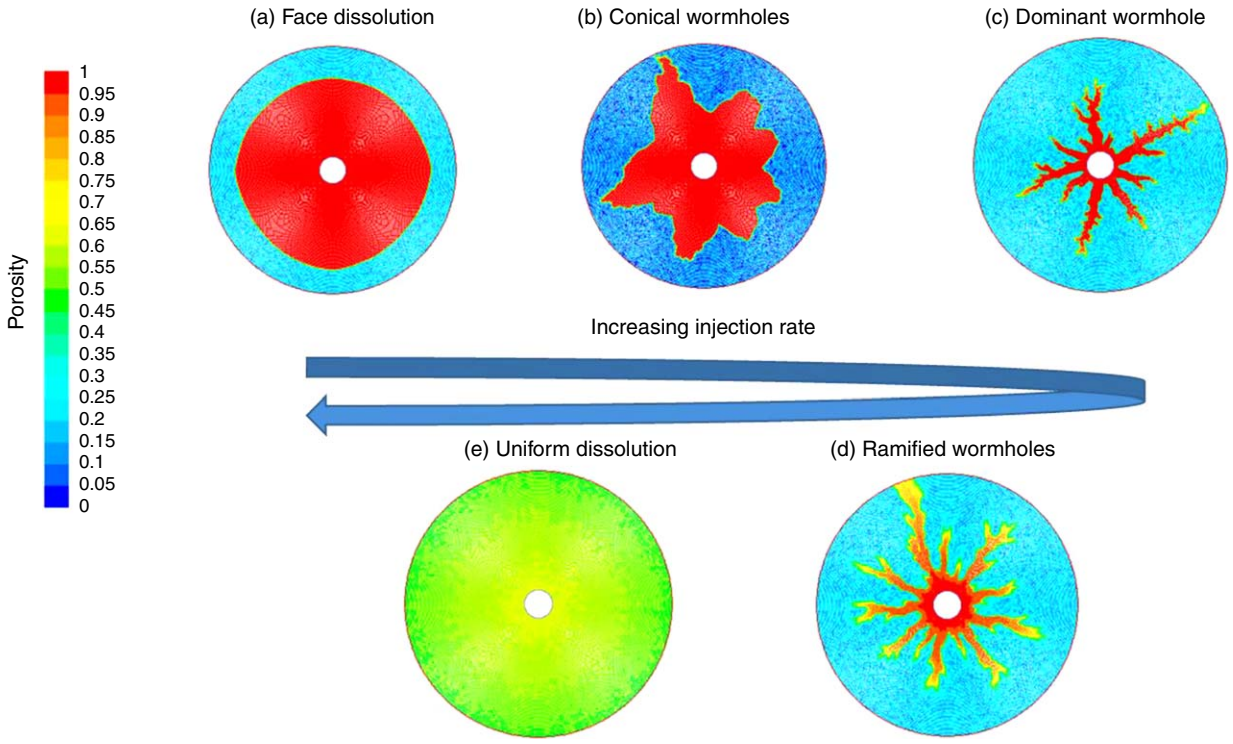

Fig. 7—Porosity contour showing the dissolution patterns obtained from injection rates ranging from a minimum of 3.23×10^{-6} m/s to a maximum of 0.323 m/s (to capture all possible dissolution patterns) from the 2D radial-flow model.

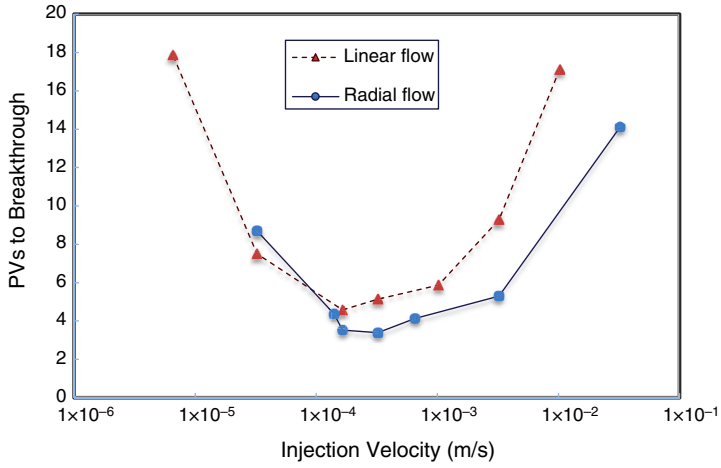

Fig. 8—Comparison of the acid-efficiency curve of the linear- and radial-flow 2D cases shows that the optimal injection rate is higher for the radial case, with a lower volume of acid required to reach breakthrough.

The largest difference in PV_{BT} is observed at the injection rate of approximately 3.0 cm^3/min, which is the ramified (highly branched) wormhole regime in which the effect of the porosity distribution is most magnified. The highest PV_{BT} value at this exact injection rate is 5.68 and the lowest is 5.16, which gives a percentage difference of 9%. At very-low injection rates, conical wormholes are formed in which the acid dissolves a large part of the rock matrix before propagating, thus considerably reducing the effect of porosity distribution on amount of acid injected to breakthrough.

Effect of Porosity Heterogeneity. The influence of medium heterogeneity on wormholing and PV_{BT} is examined here. Cases with porosity heterogeneity ranging from 0.5 to 0.95% of average porosity were simulated. The wormholes become thinner and more branched as the heterogeneity of the medium increases **(Fig. 13). Fig. 14** presents the acid-efficiency curves of the various cases simulated with different heterogeneity-magnitude values, and **Fig. 15** shows the effect of heterogeneity magnitude on PV_{BT} at the optimal injection rate.

The difference in the PV_{BT} values for the various heterogeneity cases is pronounced in the wormholing regime, but not as much as in the face- and uniform-dissolution regime (Fig. 14). In the uniform-dissolution regime, the PV_{BT} slowly decreases as the porosity-heterogeneity magnitude increases. At high heterogeneity magnitude, ramified wormholes tend to form (instead of uniform dissolution) more than they would at a lower heterogeneity magnitude with the same injection rate, resulting in a reduced amount of acid required for breakthrough.

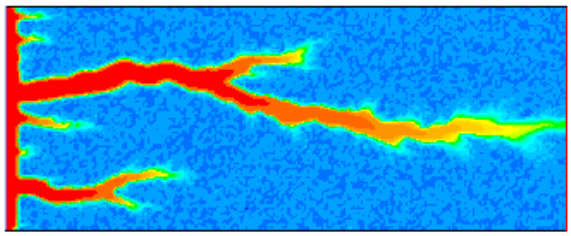

(a) $\varepsilon_o = 0.1$

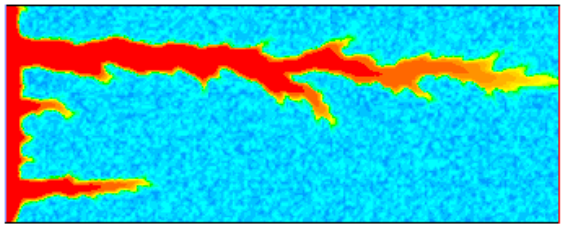

(b) $\varepsilon_o = 0.2$

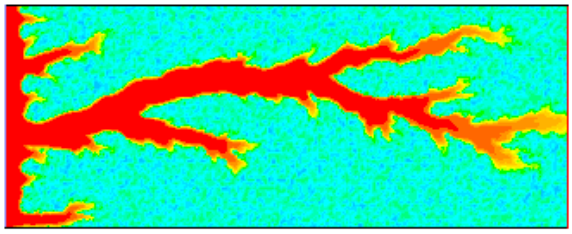

(c) $\varepsilon_o = 0.3$

Fig. 9—Effect of initial average porosity on wormhole patterns (formed at an injection rate of 1.5 cm^3/min).

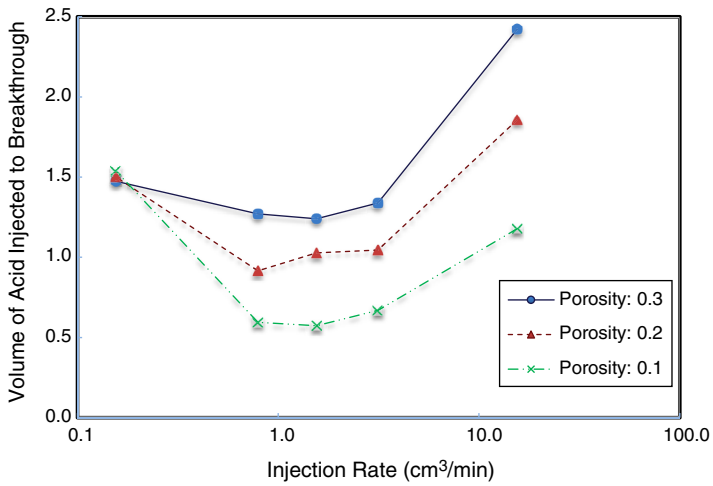

Fig. 10—Acid-efficiency curves showing the effect of initial average porosity on the amount of acid injected to reach breakthrough.

At the optimal injection rate, Fig. 15 shows that the PV_{BT} will be high for cases with very-low heterogeneity magnitude. For a rock with very-low heterogeneity, the dissolution process resembles that of face dissolution at the initial stage before branching occurs, and an additional amount of acid will be consumed in the dissolution of the face of the rock (Fig. 13a). Another reason for high PV_{BT} values for cases with low heterogeneity magnitude is that the diameter of the wormholes is thicker and less branched, also requiring more acid for propagation.

The simulation results show that PV_{BT} decreases with an increase in porosity-heterogeneity magnitude (Fig. 15) until a critical value ($\Delta\varepsilon_c = \pm 0.05$) is reached, after which higher heterogeneity values have no effect on the PV_{BT} at this optimal injection rate.

Effect of Vugs (Large-Scale Heterogeneities). To study the effect of vugs on wormholing in carbonates, the initial porosity profile was modified according to vuggy-carbonate-characterization results from the nuclear-magnetic-resonance study conducted by Vik et al. (2007). A case with total initial average porosity of 0.3 is designed with random vugs in the medium that account for 65% of the total porosity. The vugs are assigned porosity values of 0.9, and the matrix-porosity values vary between 0.15 and 0.45. **Fig. 16a** shows the initial porosity profile with random distribution of vugs in the 2D domain, and Fig. 16b presents the wormhole patterns in the form of the porosity-contour profile after simulation of coreflood injection at an optimal rate.

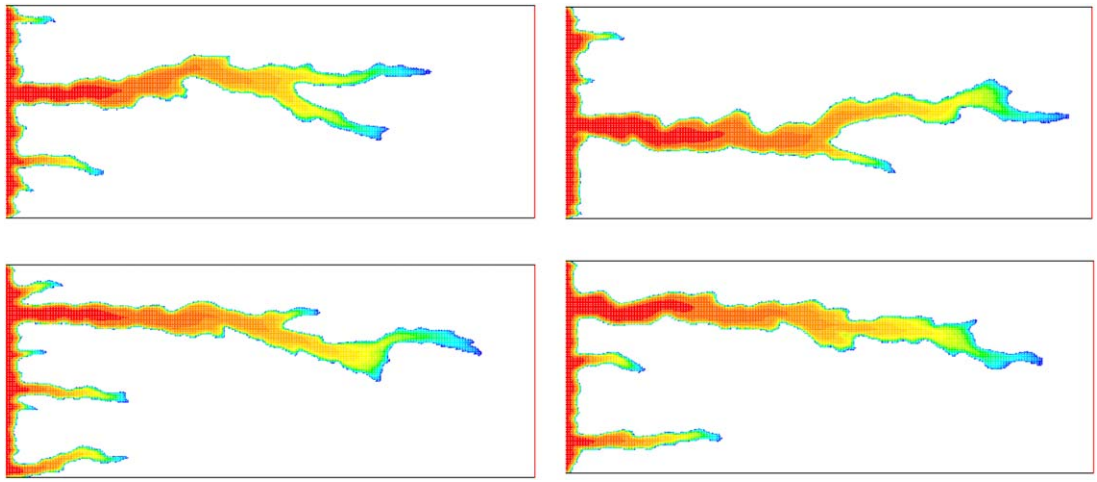

Fig. 11—Different wormhole patterns formed at an injection rate of 1.5 cm^3/min in simulated carbonate sample with same porosity (0.2) and heterogeneity magnitude (50%), but different porosity distribution.

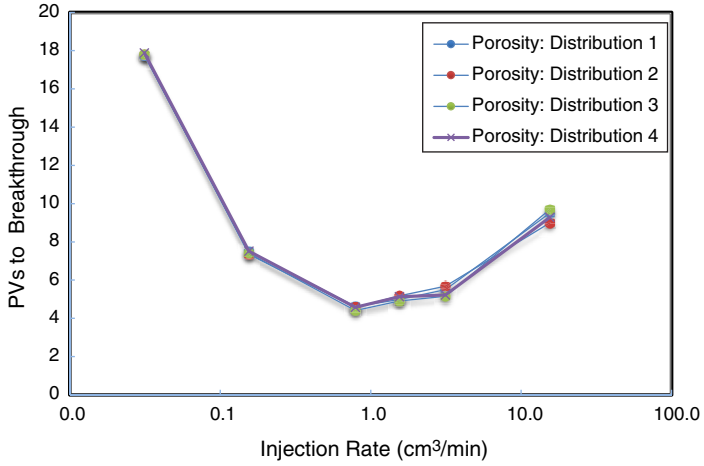

Fig. 12—Acid-efficiency curves showing the effect of porosity distribution on the PVs of acid required to reach breakthrough.

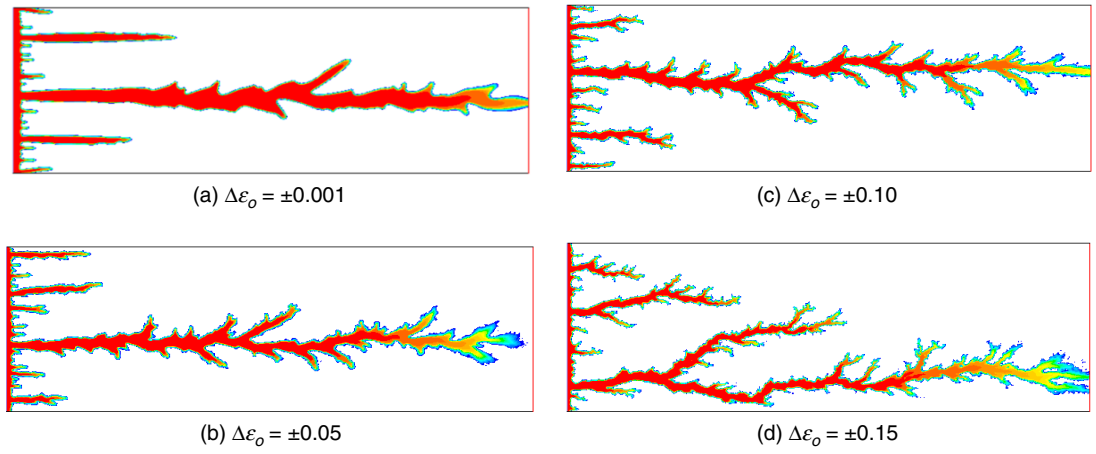

Fig. 13—Dissolution structures showing the effect of porosity-heterogeneity magnitude on the wormhole patterns at the same optimal injection rate.

Results show that acid propagates faster in the vuggy medium than in the uniform heterogeneous-porosity medium. This flow trend is evident in the plot given in **Fig. 17** comparing the acid-efficiency curves of both carbonate mediums with different heterogeneity scales. The wormhole diameter is determined by the diameter of the vug in its path. The amount of acid required to reach breakthrough in the vuggy-carbonate core is lower than that of a nonvuggy carbonate, which is in agreement with experimental results reported by Izgec et al. (2010). Their experimental and numerical work also showed that the local pressure drops created by vugs determined the wormhole-flow path. The PV_{BT} value in the vuggy medium is dependent on the positions, amount, and connectivity of vugs.

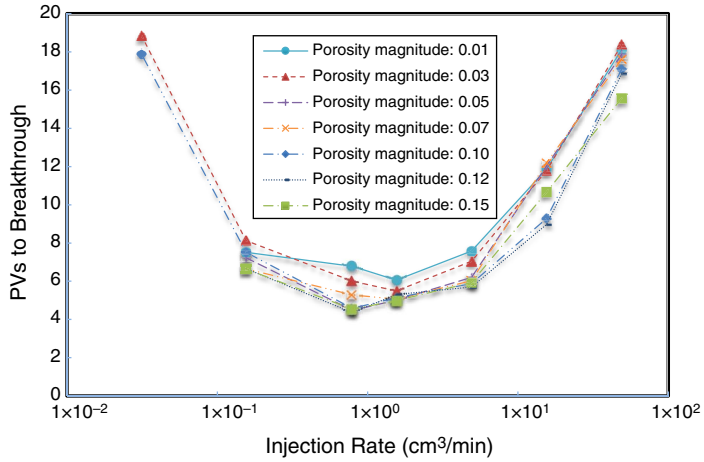

Fig. 14—Acid-efficiency curves showing the effect of porosity-heterogeneity magnitude on the PVs of acid required to reach breakthrough.

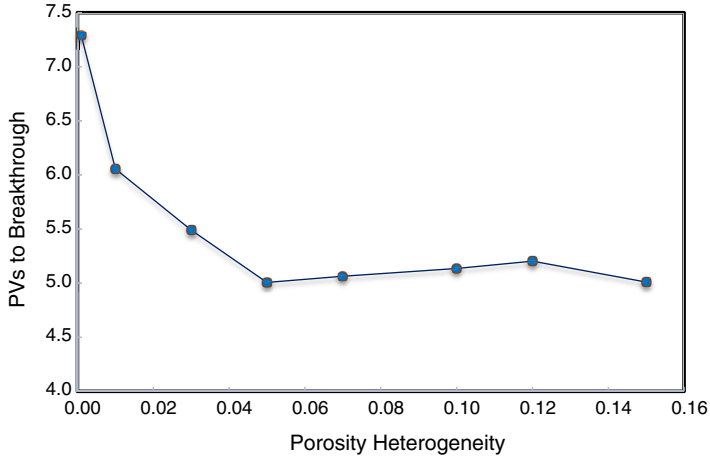

Fig. 15—Effect of porosity heterogeneity on PVs to breakthrough at the optimal injection rate.

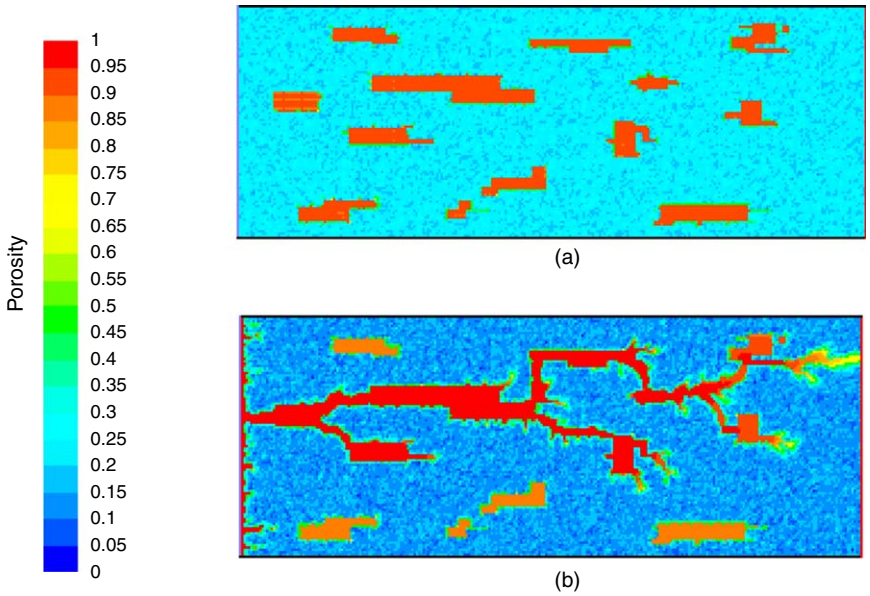

Fig. 16—Porosity-contour profile showing (a) initial porosity profile of vuggy-carbonate core and (b) wormhole patterns formed with acid injected at an optimal rate in the vuggy-carbonate core.

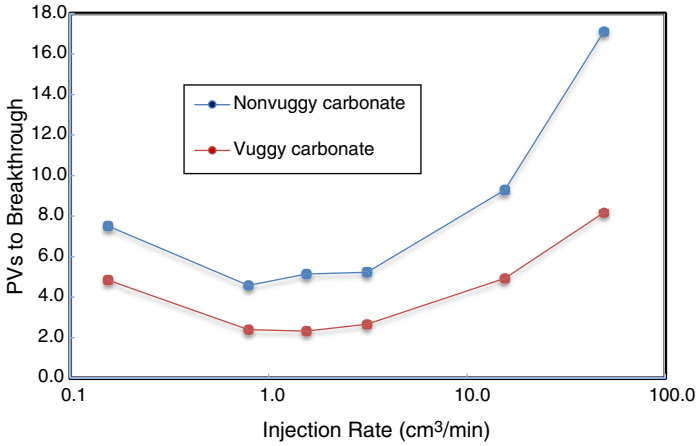

Fig. 17—Acid-efficiency curves showing the effect of large-scale heterogeneities (vugs) on the PVs of acid required to breakthrough.

Effect of Medium Dimension. Various mesh domains for the 2D model have been developed to study the effect of the aspect ratio (core dimensions) on the acid-efficiency curve. The aspect ratio is defined as the ratio of the height of the domain to its length. The dimensions of the domains and corresponding aspect-ratio values used in this study are shown in **Fig. 18.** The maximum core length investigated is 1.574 in. because of computational limitations. An extremely high number of grid cells will be required to simulate conical and face dissolution in core lengths of 6 and 20 in., used in experimental work by Furui et al. (2012) to study the effect of core dimensions on wormhole propagation.

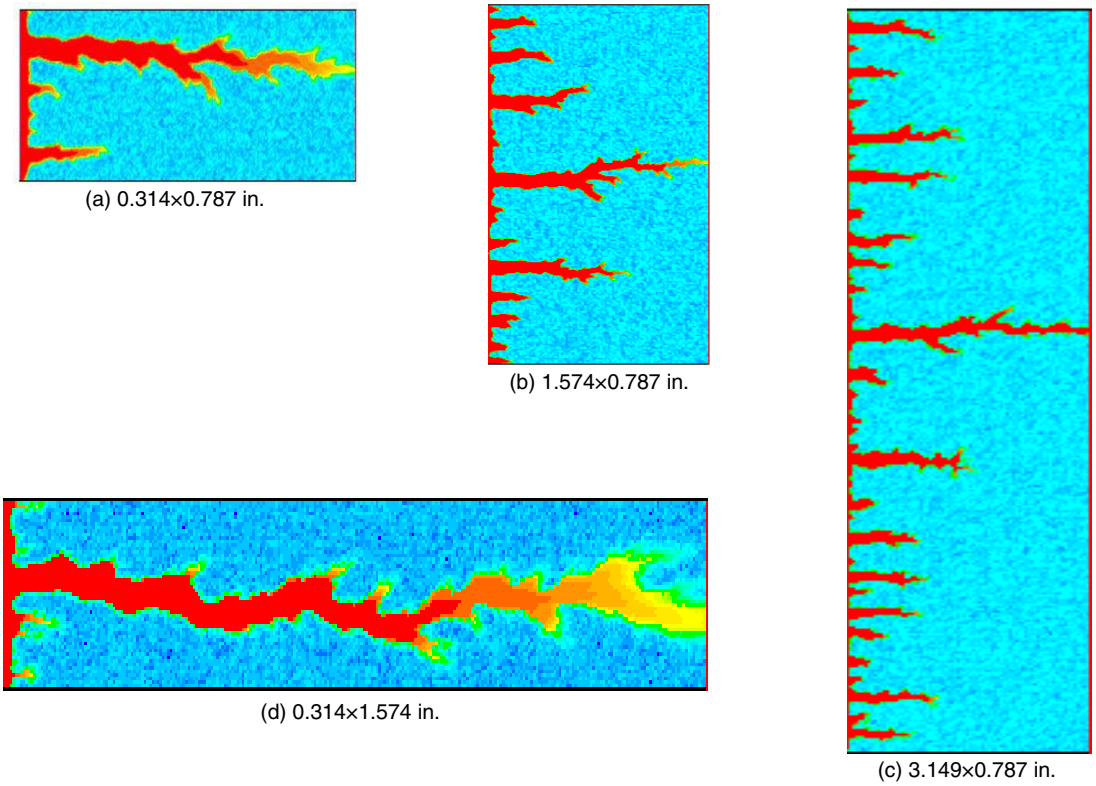

Fig. 18—Wormhole patterns for cores with various dimensions with the following aspect ratios (ARs): (a) AR = 0.4, (b) AR = 2, (c) AR = 4, (d) AR = 0.2.

The first set of results presented in **Fig. 19a** show that the value of the optimal injection rate is higher for the long core. The longer the acid propagates in the domain before reaching breakthrough at the outlet, the more the acid is consumed at the walls of the wormhole; therefore, a higher optimal injection rate will be required to transport the acid to the tips of dominant wormholes for longer domains. This trend is in agreement with the conclusion of experimental studies on the effect of core length on the acid-efficiency curve by Bazin (2001).

Fig. 19b shows the results of the effect of the domain height (core diameter) on the acid-efficiency curve. The plot shows that PV_{BT} in the wormhole regimes is inversely proportional to the height of the domain. It can be seen from Fig. 18 that the number of wormholes started at the injection inlet increases with the height of the domain, but only one dominant wormhole reaches the outlet. This means that the fractional amount of the solid phase to be dissolved for the acid to reach breakthrough is reduced with an increase in the domain

height. At very-high injection rates, the PV_{BT} does not depend on the height of the domain because the amount of acid required to reach breakthrough increases proportionally with domain height because of the uniform dissolution of the solid phase. These results are consistent with experimental studies by Furui et al. (2012) on the effect of core diameter on amount of acid injected to breakthrough.

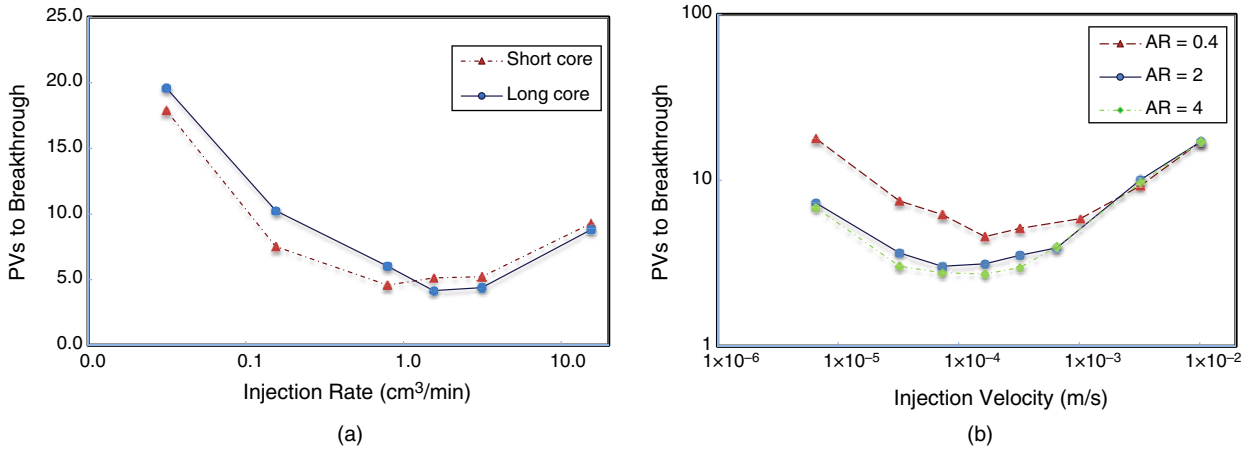

Fig. 19—(a) Numerical-model results showing the effect of core length on the acid-efficiency curve (short core length = 0.787 in. and long core length = 1.574 in.). (b) Simulation results showing the effect of the core AR on the acid-efficiency curve [length of core is fixed at 0.787 in.; diameters of the three cases are 0.314 in. (AR = 0.4), 1.574 in. (AR = 2), and 3.149 in. (AR = 4)].

Effect of Reaction Kinetics. The sensitivity of the model to reaction-rate constant and order of reaction, with resulting effect on optimal injection rate and PV_{BT} values, is demonstrated and discussed in this subsection.

Reaction-Rate Constant. Three cases with different reaction-rate constants were simulated, and **Fig. 20** presents the resulting acid-efficiency curves. To reach the dominant wormhole regime, the faster-reacting acid will have to be injected at a higher rate than a slower-reacting acid for most of the acid to be transported to the tips of the wormholes and not be totally consumed along the walls of the wormholes. Previous experimental studies have shown that wormholes created by fast-reacting acids are thinner and more branched than those created by slow-reacting acids. This leads to lower PV_{BT} values and higher optimal injection rates at the wormhole regimes for acid/mineral systems with higher rates of reaction. This trend in Fig. 20 is similar to that observed in the experimental study by Furui et al. (2012) on how the overall rate of reaction affects the acid-efficiency curve.

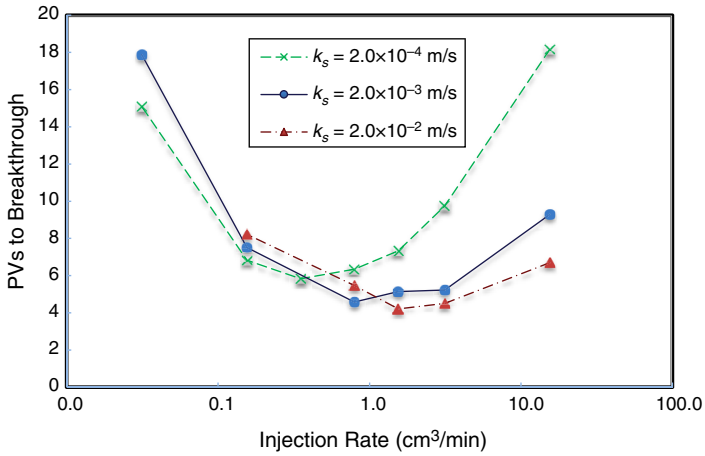

Fig. 20—Numerical-model results showing the effect of reaction-rate constant on the acid-efficiency curve.

Order of Reaction. In the cases presented so far for this simulation study, linear first-order kinetics are assumed, and the output has been shown in the previous subsection to agree qualitatively with experimental results of previous investigations. Here, a nonlinear reaction-kinetics model is used in which $R(C) = k_s C_s^n$, where n is the order of reaction. The simulation results showing the effect of the order of reaction are presented in **Fig. 21.** The higher the order of reaction, the lower the optimal injection rate and amount of acid required to reach breakthrough. As noted by Maheshwari et al. (2012), there is no agreement in the literature regarding the magnitude of reaction-rate constant and order of reaction, but the present simulation results show that the order of reaction significantly influences PV_{BT} values.

Conclusions

In this study, a new modified two-scale model has been used to investigate and quantify wormhole propagation during carbonate acidizing by use of the Navier-Stokes approach. The outputs from this model were compared with experimental results and previous models in the literature, and the following conclusions stem from the numerical simulations:

1. The Navier-Stokes momentum approach can be used to effectively describe fluid flow in a two-scale model, and the modified model in this work captures all the dissolution patterns that occur during carbonate-matrix acidizing.
2. Sensitivity tests conducted on the model for various factors that affect wormhole propagation during carbonate acidizing provided results consistent with experimental observations and previous two-scale models with flow field given by Darcy's law.
3. At dissolution regimes above the optimal injection rate, the computational time by use of the Navier-Stokes approach is significantly lower than the reported computational time for models derived from Darcy's law.
4. The simulation results from this study show that the geometry of flow affects the dissolution process and determines the optimal injection rate with the amount of acid required to reach breakthrough. Thus, the linear flow modeled in laboratory experiments is not representative of radial flow that occurs in field conditions.
5. The effects of initial average porosity and formation heterogeneity on the PVs of acid injected to breakthrough in a coreflood experiment were presented from the simulation output. The model also showed how the core dimensions influence the optimal injection rate and PVs of acid injected to reach breakthrough in coreflood experiments. This dimension should be accounted for in the translation of optimal injection rates obtained from coreflood experiments to field applications.
6. Reaction-rate kinetics influence the wormholing process, as the model demonstrates. The optimal injection rate increases as the reactivity of the acid, in the form of the reaction-rate constant, increases, and the amount of acid required to reach breakthrough is reduced.
7. The introduction of nonlinear kinetics illustrates the significant influence of fractional orders of reaction on the optimal injection rate and the amount of acid required to reach breakthrough. It also shows the possibility of extending the two-scale model to alternative acidizing fluids such as chelants and organic acids, which will require further modification to handle reversible surface reactions.

This work has shown that fluid flow in a two-scale model can be effectively described by the Navier-Stokes momentum approach. The order of reaction is demonstrated to significantly influence the PVs of acid injected to breakthrough in the model, which is relevant in the extension of the two-scale model for alternative acidizing fluids.

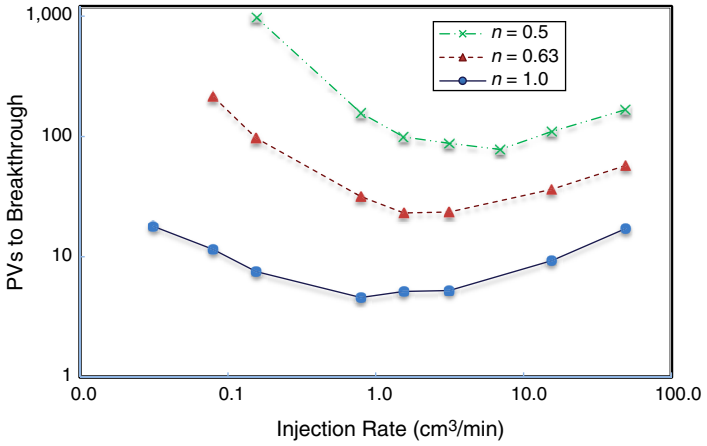

Fig. 21—Numerical-model results showing the effect of order of reaction on the acid-efficiency curve.

Nomenclature

$\boldsymbol{a_o}$ = initial interfacial area per unit volume of the medium, 1/L, m^{-1}
$\boldsymbol{a_v}$ = interfacial area per unit volume of the medium, 1/L, m^{-1}
C_f = original concentration of acid in the fluid phase, n/L^3, mol/L
C_s = concentration of acid at the solid/fluid interface, n/L^3, mol/L
C_2 = inertial-resistance factor
$\boldsymbol{D_e}$ = effective dispersion tensor, L^2/t, m^2/s
D_{eT} = effective transverse-dispersion coefficient, L^2/t, m^2/s
D_{eX} = effective longitudinal-dispersion coefficient, L^2/t, m^2/s
D_m = acid diffusivity, L^2/t, m^2/s
F = sum of external body forces and source terms in momentum equation, m/L^2t^2, $kg/m^2 \cdot s^2$
g = acceleration caused by gravity, L/t^2, m/s^2
k_c = local mass-transfer coefficient, L/t, m/s
$\mathbf{K}$ = permeability tensor, L^2, m^2
$\mathbf{K_o}$ = initial permeability tensor, L^2, m^2
k_s = surface-dissolution reaction-rate constant, L/t, m/s
n = order of reaction
PV_{BT} = PVs of acid injection to breakthrough
Q = acid-injection rate, L^3/t, m^3/s
$\boldsymbol{r_o}$ = initial pore radius, L, m
$\boldsymbol{r_p}$ = pore radius, L, m
$R(C)$ = reaction kinetics, $n/t/L^2$, $mol/s/m^2$
Re_p = Reynolds number
S = momentum source term, m/L^2t^2, kg/m^2s^2
Sc = Schmidt number
Sh = Sherwood number
Sh_∞ = asymptotic Sherwood number
S_m = source mass added to continuity equation, m, kg

$\mathbf{u}$ = superficial velocity vector, L/t, m/s
α = dissolving power of acid, m/n, g/mol
α_{os} = constant in dispersion correlations
β = pore-structure-relation constant
$\Delta\varepsilon$ = porosity-heterogeneity magnitude
$\Delta\varepsilon_c$ = critical porosity-heterogeneity magnitude
ε = porosity of the porous medium
ε_o = initial porosity
λ_T = constant in transverse-dispersion correlation
λ_X = constant in axial-dispersion correlation
μ = fluid viscosity, m/Lt, mPa·s
ν = kinematic viscosity, L^2/t, m^2/s
ρ = fluid density, m/L^3, kg/m^3
ρ_s = rock density, m/L^3, kg/m^3
$\boldsymbol{\tau}$ = stress tensor, m/Lt^2, psi [MPa]

Acknowledgments

The authors would like to thank Carbo Ceramics Incorporated for providing financial support for this study and permission to publish this paper. The authors also recognize Gia Alexander for assistance in preparing the manuscript.

References

ANSYS. 2015. ANSYS Fluent, Version 15.0. Canonsburg, Pennsylvania: ANSYS, Incorporated.

Akanni, O. O. and Nasr-El-Din, H. A. 2015. The Accuracy of Carbonate Matrix-Acidizing Models in Predicting Optimal Injection and Wormhole Propagation Rates. Presented at the SPE Middle East Oil & Gas Show and Conference, Manama, Bahrain, 8–11 March. SPE-172575-MS. https://doi.org/10.2118/172575-MS.

Balakotaiah, V. and West, D. H. 2002 Shape Normalization and Analysis of Mass Transfer Controlled Regime in Catalytic Monoliths. *Chem. Eng. Sci.* **57** (8): 1269–1286. https://doi.org/10.1016/S0009-2509(02)00059-3.

Bazin, B. 2001. From Matrix Acidizing to Acid Fracturing: A Laboratory Evaluation of Acid/Rock Interactions. *SPE Prod & Fac* **16** (1): 22–29. SPE-66566-PA. https://doi.org/10.2118/66566-PA.

Bryant, S. L., Mellor, D. W., and Cade, C. A. 1993. Physically Representative Network Models of Transport in Porous Media. *AIChE J.* **39** (3): 387–396. https://doi.org/10.1002/aic.690390303.

Buijse, M. A. 2000. Understanding Wormholing Mechanisms Can Improve Acid Treatments in Carbonate Formations. *SPE Prod & Oper* **15** (3): 168–175. SPE-38166-MS. https://doi.org/10.2118/38166-MS.

Buijse, M. A. and Glasbergen, G. 2005. A Semi-Empirical Model to Calculate Wormhole Growth in Carbonate Acidizing. Presented at the SPE Annual Technical Conference and Exhibition, Dallas, 9–12 October. SPE-96892-MS. https://doi.org/10.2118/96892-MS.

Carman, P. C. 1937. Fluid Flow Through Granular Beds. *Transactions - Institution of Chemical Engineers* **15:** 150–166.

Cohen, C. E., Ding, D., Quintard, M. et al. 2008. From Pore Scale to Wellbore Scale: Impact of Geometry on Wormhole Growth in Carbonate Acidization. *Chem. Eng. Sci.* **63** (12) 3088–3099. https://doi.org/10.1016/j.ces.2008.03.021.

Daccord, G., Touboul, E., and Lenormand, R. 1989. Carbonate Acidizing: Toward a Quantitative Model of the Wormholing Phenomenon. *SPE Prod Eng* **4** (1): 63–68. SPE-16887-PA. https://doi.org/10.2118/16887-PA.

De Oliveira, T. J. L., De Melo, A. R., Oliveira, J. A. et al. 2012. Numerical Simulation of the Acidizing Process and PVBT Extraction Methodology Including Porosity/Permeability and Mineralogy Heterogeneity. Presented at the SPE International Symposium and Exhibition on Formation Damage Control. Lafayette, Louisiana, 15–17 January. SPE-151823-MS. https://doi.org/10.2118/151823-MS.

Fatt, I. 1956. The Network Model of Porous Media. Published in *Petroleum Transactions,* AIME, Vol. 207, 144–181. SPE-574-G.

Fredd, C. N. and Fogler, H. S. 1998. Influence of Transport and Reaction on Wormhole Formation in Porous Media. *AIChE J.* **44** (9): 1933–1949. https://doi.org/10.1002/aic.690440902.

Fredd, C. N. and Fogler, H. S. 1999. Optimal Conditions for Wormhole Formation in Carbonate Porous Media: Influence of Transport and Reaction. *SPE J.* **4** (3): 196–205. SPE-56995-PA. https://doi.org/10.2118/56995-PA.

Fredd, C. N. and Miller, M. J. 2000. Validation of Carbonate Matrix Stimulation Models. Presented at the SPE International Symposium on Formation Damage Control, Lafayette, Louisiana, 23–24 February. SPE-58713-MS. https://doi.org/10.2118/58713-MS.

Frick, T. P., Kurmayr, M., and Economides, M. J. 1994. An Improved Modeling Of Fractal Patterns in Matrix Acidizing and Their Impact on Well Performance. *SPE Prod & Oper* **9** (1): 61–68. SPE-23789-PA. https://doi.org/10.2118/23789-PA.

Furui, K., Burton, R., Burkhead, D. et al. 2012. A Comprehensive Model of High-Rate Matrix-Acid Stimulation for Long Horizontal Wells in Carbonate Reservoirs: Part I–Scaling Up Core-Level Acid Wormholing to Field Treatments. *SPE J.* **17** (1): 271–279. SPE-134265-PA. https://doi.org/10.2118/134265-PA.

Ghommem, M. and Brady, B. 2015. Multifidelity Modeling and Analysis of Matrix Acidizing under Radial Flow Conditions. Oral presentation given at the International Petroleum Technology Conference, Doha, Qatar, 6–9 December.

Ghommem, M., Zhao, W., Dyer, S. et al. 2015. Carbonate Acidizing: Modeling, Analysis, and Characterization of Wormhole Formation and Propagation. *J. Pet. Sci. Eng.* **131** (July): 18–33. https://doi.org/10.1016/j.petrol.2015.04.021.

Glasbergen, G., Kalia, N., and Talbot, M. S. 2009. The Optimal Injection Rate for Wormhole Propagation: Myth or Reality?. Presented at the 8th European Formation Damage Conference, Scheveningen, The Netherlands, 27–29 May. SPE-121464-MS. https://doi.org/10.2118/121464-MS.

Golfier, F., Zarcone, C., Bazin, B. et al. 2002. On the Ability of a Darcy-Scale Method Model To Capture Wormhole Formation During the Dissolution of a Porous Medium. *J. Fluid Mech.* **457** (April): 213–254. https://doi.org/10.1017/S0022112002007735.

Gupta, N. and Balakotaiah, V. 2001. Heat and Mass Transfer Coefficients in Catalytic Monoliths. *Chem. Eng. Sci.* **56** (16): 4771–4786. https://doi.org/10.1016/S0009-2509(01)00134-8.

Hoefner, M. L. and Fogler, H. S. 1988. Pore Evolution and Channel Formation During Flow and Reaction in Porous Media. *AIChE J.* **34** (1): 45–54. https://doi.org/10.1002/aic.690340107.

Huang, T., Hill, A. D., and Schechter, R. S. 1997. Reaction Rate and Fluid Loss: The Keys to Wormhole Initiation and Propagation in Carbonate Acidizing. Presented at the International Symposium on Oilfield Chemistry, Houston, 18–21 February. SPE-37312-MS. https://doi.org/10.2118/37312-MS.

Hung, K. M., Hill, A. D., and Sepehrnoori, K. 1989. A Mechanistic Model of Wormhole Growth in Carbonate Matrix Acidizing and Acid Fracturing. *J Pet Technol* **41** (1): 59–66. SPE-16886-PA. https://doi.org/10.2118/16886-PA.

Izgec, O., Zhu, D., and Hill, A. D. 2010. Numerical and Experimental Investigation of Acid Wormholing during Acidization of Vuggy Carbonate Rocks. *J. Pet. Sci. Eng.* **74** (1): 51–66. https://doi.org/10.1016/j.petrol.2010.08.006.

Kalia, N. and Balakotaiah, V. 2007. Modeling and Analysis of Wormhole Formation in Reactive Dissolution of Carbonate Rocks. *Chem. Eng. Sci.* **62** (4): 919–928. https://doi.org/10.1016/j.ces.2006.10.021.

Kalia, N. and Balakotaiah, V. 2009. Effect of Medium Heterogeneities on Reactive Dissolution of Carbonates. *Chem. Eng. Sci.* **64** (2): 376–390. https://doi.org/10.1016/j.ces.2008.10.026.

Kalia, N. and Glasbergen, G. 2009. Wormhole Formation in Carbonates under Varying Temperature Conditions. Presented at the 8th SPE European Formation Damage Conference. Scheveningen, The Netherlands, 27–29 May. SPE-121803-MS. https://doi.org/10.2118/121803-MS.

Liu, M., Zhang, S., and Mou, J. 2012. Effect of Normally Distributed Porosities on Dissolution Pattern in Carbonate Acidizing. *J. Pet. Sci. Eng.* **94–95** (September): 28–39. https://doi.org/10.1016/j.petrol.2012.06.021.

Liu, X., Ormond, A., Bartko, K. et al. 1997. A Geochemical Reaction-Transport Simulator for Matrix Acidizing Analysis and Design. *J. Pet. Sci. Eng.* **17** (1–2): 181–196. https://doi.org/10.1016/S0920-4105(96)00064-2.

Maheshwari, P. and Balakotaiah, V. 2013. Comparison of Carbonate HCl Acidizing Experiments with 3D Simulations. *SPE Prod & Oper* **28** (4): 402–413. SPE-164517-PA. https://doi.org/10.2118/164517-PA.

Maheshwari, P., Maxey, J., and Balakotaiah, V. 2014. Simulation and Analysis of Carbonate Acidization with Gelled and Emulsified Acids. Presented at the Abu Dhabi International Petroleum Exhibition and Conference, Abu Dhabi, 10–13 November. SPE-171731-MS. https://doi.org/10.2118/171731-MS.

Maheshwari, P., Ratnakar, R. R., Kalia, N. et al. 2012. 3-D Simulation and Analysis of Reactive Dissolution and Wormhole Formation in Carbonate Rocks. *Chem. Eng. Sci.* **90** (7 March): 258–274. https://doi.org/10.1016/j.ces.2012.12.032.

Panga, M. K. R., Ziauddin, M., and Balakotaiah, V. 2005. Two-Scale Continuum Model for Simulation of Wormholes in Carbonate Acidization. *AIChE J.* **51** (12): 3231–3248. https://doi.org/10.1002/aic.10574.

Panga, M. K. R., Balakotaiah, V., and Ziauddin, M. 2002. Modeling, Simulation and Comparison of Models for Wormhole Formation during Matrix Stimulation of Carbonates. Presented at the SPE Annual Technical Conference and Exhibition, San Antonio, Texas, 29 September–2 October. SPE-77369-MS. https://doi.org/10.2118/77369-MS.

Ratnakar, R. R., Kalia, N., and Balakotaiah, V. 2012. Carbonate Matrix Acidizing with Gelled Acids: An Experiment-Based Modeling Study. Presented at the SPE International Production and Operations Conference and Exhibition, Doha, Qatar, 14–16 February. SPE-154936-MS. https://doi.org/10.2118/154936-MS.

Rose, W. 1957. Studies of Waterflood Performance: III. Use of Network Models. Illinois State Geological Survey, Urbana, Illinois.

Rowan, G. 1959. Theory of Acid Treatment of Calcite Formations. *J. Inst. Petrol.* **45** (431).

Sahimi, M., Gavalas, G. R., and Tsotsis, T. T. 1990. Statistical and Continuum Models of Fluid-Solid Reactions in Porous Media. *Chem. Eng. Sci.* **45** (6): 1443–1502. https://doi.org/10.1016/0009-2509(90)80001-u.

Schechter, R. S. 1992. *Oil Well Stimulation*. New York City: Prentice Hall.

Schechter, R. S. and Gidley, J. L. 1969. The Change in Pore Size Distribution from Surface Reactions in Porous Media. *AIChE J.* **15** (3): 339–350. https://doi.org/10.1002/aic.690150309.

Simon, R. and Kelsey, F. J. 1972. The Use of Capillary Tube Networks in Reservoir Performance Studies: II. Effect of Heterogeneity and Mobility on Miscible Displacement Efficiency. *SPE J.* **12** (4): 345–351. SPE-3482-PA. https://doi.org/10.2118/3482-PA.

Thompson, K. E. and Fogler, H. S. 1997. Modeling Flow in Disordered Packed Beds from Pore-Scale Fluid Mechanics. *AIChE J.* **43** (6): 1377–1389. https://doi.org/10.1002/aic.690430602.

Vik, B., Djurhuus, K., Spildo, K. et al. 2007. Characterization of Vuggy Carbonates. Presented at the SPE/EAGE Reservoir Characterization and Simulation Conference, Abu Dhabi, 28–31 October. SPE-111434-MS. https://doi.org/10.2118/111434-MS.

Wang, Y., Hill, A. D., and Schechter, R. S. 1993. The Optimal Injection Rate for Matrix Acidizing of Carbonate Formations. Presented at the SPE Annual Technical Conference and Exhibition, Houston, 3–6 October. SPE 26578-MS. https://doi.org/10.2118/26578-MS.

Zhang, Y., Yang, S., Zhang, S. et al. 2014. Wormhole Propagation Behavior and Its Effect on Acid Leakoff under In Situ Conditions in Acid Fracturing. *Transport Porous Med.* **101** (1): 99–114. https://doi.org/10.1007/s11242-013-0233-z.

Olatokunbo Akanni is a well-stimulation engineer with Carbo Ceramics in Houston. Previously, he worked for 4 years as a research and teaching assistant at the Petroleum Engineering Department at Texas A&M University, and for 2 years as a research assistant at the New Mexico Petroleum Recovery Research Center. Akanni has published several technical papers, and his research interests include well stimulation, production forecasting, polymer flooding, and reservoir profile modification for waterflooding. He holds a PhD degree in petroleum engineering from Texas A&M University, a master's degree in petroleum engineering from New Mexico Institute of Mining and Technology, and a bachelor's degree in electronic and electrical engineering from Obafemi Awolowo University, Nigeria. Akanni currently serves as a question writer for the SPE PetroBowl and a mentor in the SPE eMentorship program.

Hisham A. Nasr-El-Din is a professor and holder of the John Edgar Holt Endowed Chair in Petroleum Engineering at Texas A&M University. Previously, he worked for 15 years as principal professional and team leader of the Stimulation Research and Technology Team at Saudi Aramco. Before joining Saudi Aramco, Nasr-El-Din worked for 4 years as a staff research engineer with the Petroleum Recovery Institute in Calgary. He also worked as a research associate with the University of Saskatchewan, the University of Ottawa, and the University of Alberta, all in Canada. Nasr-El-Din's research interests include well stimulation, formation damage, enhanced oil recovery, conformance control, interfacial properties, adsorption, rheology, cementing, drilling fluids, two-phase flow, and nondamaging fluid technologies. He holds more than 30 patents, has written 15 book chapters, and has published and presented more than 650 technical papers. Nasr-El-Din has received numerous awards within Saudi Aramco for significant contributions in stimulation and treatment-fluid technologies and stimulation design, and for his work in training and mentoring. He holds bachelor's and master's degrees from Cairo University, Egypt, and a PhD degree from the University of Saskatchewan, Canada, all in chemical engineering. Nasr-El-Din is a review chairperson for *SPE Journal*, and is a technical editor for *SPE Production & Operations* and *SPE Drilling & Completion*. He has been invited to give keynote presentations in various SPE and National Association of Corrosion Engineers conferences. Nasr-El-Din received the SPE Regional Technical Discipline Award for Production and Operations in 2006, was named an SPE Distinguished Member in 2007, and received SPE awards for Outstanding Associate Editor (*SPE Journal*) and Outstanding Technical Editor (*SPE Production & Operations*) in 2008. In addition, he received the SPE Production and Operations Award and SPE Outstanding Associate Editor Award (*SPE Journal*) in 2009. Nasr-El-Din received SPE A Peer Apart status in 2011 for reviewing more than 100 papers. He was the recipient of the 2013 SPE Distinguished Achievement Award for Petroleum Engineering Faculty.

Deepak Gusain is a senior engineer with Carbo Ceramics in Houston, with more than 13 years of product-development experience. Before joining Carbo, he worked for Weatherford, where he helped develop several reservoir-monitoring systems. Gusain has authored or coauthored several SPE papers. He holds a bachelor's degree in computer engineering from IP University, India.